Transactions, SMiRT-22
San Francisco, California, USA - August 18-23, 2013
Division I

A QUANTITATIVE INVESTIGATION OF THE EFFECTS OF LOAD INDUCED THERMAL STRAIN ON CONCRETE MICROSTRUCTURE

Robert Stein[1,2], Mihail Petkovski[2] and Dirk L. Engelberg[3]

[1]Student, Nuclear FiRST Doctoral Training Centre, University of Sheffield/University of Manchester, UK
[2]Lecturer, Department of Civil and Structural Engineering, University of Sheffield, UK
[3]Lecturer, Research Centre for Radwaste and Decommissioning & Materials Performance Centre, School of Materials, University of Manchester, UK

ABSTRACT

A quantitative microstructural investigation was carried out to determine the presence of changes in the porous volume of specimens which had been subjected to Load Induced Thermal Strain (LITS) – an irreversible strain component which occurs in mature ordinary Portland cement based materials that are heated under the presence of mechanical load. The results of mercury intrusion porosimetry and back-scattered electron image analysis indicate that the porous volume of LITS affected specimens after heating and loading is similar to that of specimens which had experienced heat only treatments. Therefore the presence of a specific microstructural damage mechanism which accounts for the development of LITS is partly discounted in the pore structure range >0.02 μm in equivalent diameter considered here. However, an increase in the variability of mercury intrusion results for affected specimens over that of heat only and control specimens and changes in pore size distribution indicates a variation in heterogeneity of material microstructure that requires further investigation.

INTRODUCTION

Load Induced Thermal Strain (LITS) is an irreversible strain component which occurs in addition to creep and elastic strain when a mature Ordinary Portland Cement (OPC) based concrete is subjected to mechanical load during first heating. Under a significant pre-stressing force, LITS is capable of completely suppressing thermal expansion in the loaded axes (Anderberg & Thelandersson, 1976) and is known to cause a significant alteration in the strength and stiffness of concrete structures (Khoury, 1992 and Petkovski, 2010). OPC based materials are employed in safety critical reactor infrastructure such as the pre-stressed reactor pressure vessel of Advanced Gas-cooled Reactors (AGR), which may experience temperatures of up to 250 ^{o}C during Loss of Coolant Accidents (LoCA).

Currently, the microstructural processes which underlie LITS remain undiscovered. An improved knowledge of the influence of LITS on concrete microstructure is necessary to enable the validation and improvement of existing numerical models to ensure adequate structural performance and durability of reactor designs. One hypothesis is that LITS is a result of moisture movement between micro-pores in the cement gel and capillary pores which leads to Load Induced Thermal Damage (LITD) (Petkovski, 2010). Damage to the solid structure of the cement caused by moisture “micro-diffusion” between gel and capillary pores was initially used to describe the microstructural origins of the Pickett effect (drying creep) alone (Hansen & Eriksson, 1966 and Bazant & Chern, 1985). The mechanism thought to be driving this micro-diffusion was the existence of a thermodynamic imbalance between water in gel pores and capillary pores during a finite period of time following hydration (Bazant & Chern, 1985). The LITD hypothesis is based on an assumption that the presence of an external compressive load would restrict moisture transfer between gel pores and capillary pores that is driven by the increase in temperature causing incremental microstructural damage which would be dependent on the magnitude of mechanical and thermal load applied.

This paper aims to investigate the presence of LITD through microstructural analysis of typical AGR pressure vessel concrete specimens using scanning electron microscopy and Mercury Intrusion Porosimetry (MIP). The study focuses on the determination of changes in the capillary pore volume in LITS affected specimens, which may be concurrent with the LITD theory.

EXPERIMENTAL SETUP AND METHODOLOGY

Specimen Preparation, Curing and Conditioning

One concrete mix used to construct the Heysham 2 AGR pressure vessel (Petkovski & Crouch 2008) was considered with all constituents and mass proportions shown in Table 1. The concrete was cast in slabs with dimensions of 740 mm x 620 mm x 150 mm and immersed in a temperature controlled water tank with a 10 day curing cycle in which the temperature reached a maximum of 65 ^{o}C. Following the 10 day cycle, the slabs were de-moulded and returned to the water tank for a further 60 days at 20 ^{o}C. The concrete had a mean uni-axial cube strength (f_{cu}) of 59MPa after 70 days. Each concrete slab was then cut and ground to form the 100 mm x 100 mm x 100 mm cubes used here. The machined cubes were stored at room temperature and humidity for ca. 3200 days before testing.

Table 1: Concrete mix proportions (OPC = Ordinary Portland cement; PFA = Pulverised fuel ash)

Constituent Name	OPC	PFA	Sand	Quartz-diorite 10 mm	Quartz-diorite 20 mm	Plasticiser SP4	Water
Cement Mass Ratio	1	0.33	2.45	1.39	2.78	0.0006	0.56
Constituent/binder mass ratio	0.75	0.25	1.84	1.05	2.16	0.0045	0.42

The experimental program consisted of six tests, with three different conditioning regimes and two repetitions for each (Table 2). The conditioning regimes included (**H250**) thermal loading only (No LITS), (**L06H250**) mechanical load followed by thermal treatment (LITS affected) and (**Control**) untreated reference specimens. All thermally treated specimens experienced a heating/cooling rate of 0.2 ^{o}C/min and all mechanical loading was hydrostatic compression. After completing the appropriate mechanical loading and/or thermal treatment, a steady state period of 24 hours was allowed before unloading/cooling. Specimen conditioning was carried out using the mac^{2T} apparatus (Petkovski *et al*. 2006) for multiaxial compression of concrete at the University of Sheffield (Figure 1).

Table 2: Conditioning regimes of the concrete cubes.

Conditioning Name	H250	L06H250	Control
Mechanical Loading	-	0.6 f_{cu}	-
Thermal Treatment	250 ^{o}C	250 ^{o}C	-

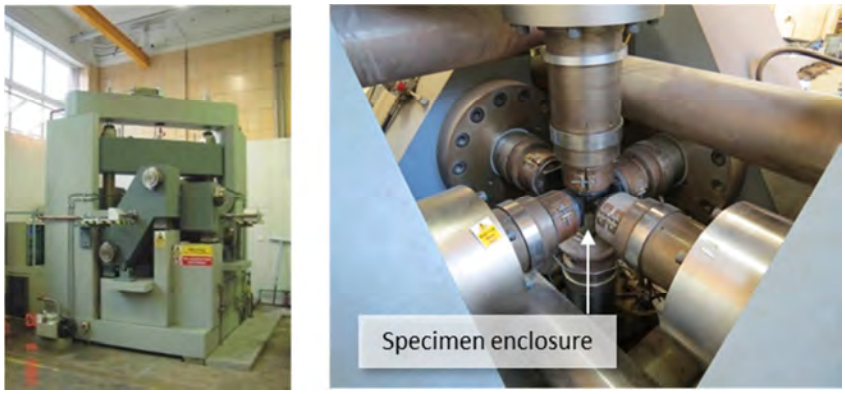

Figure 1: (left) The mac^{2T} experimental apparatus at the University of Sheffield (right) multi-axial load frame and specimen enclosure before loading.

Following conditioning, specimens were prepared for micro-structural analysis. A 25 mm core was removed from the centre of each cube, shown in Fig. 2. This core was then sectioned into ten 8 mm thick disks. The size of the disks was chosen to match the largest intrusion permeameter thimble available for MIP experiments. After cutting, all disks were sealed in plastic film and stored at room temperature to preserve internal moisture content.

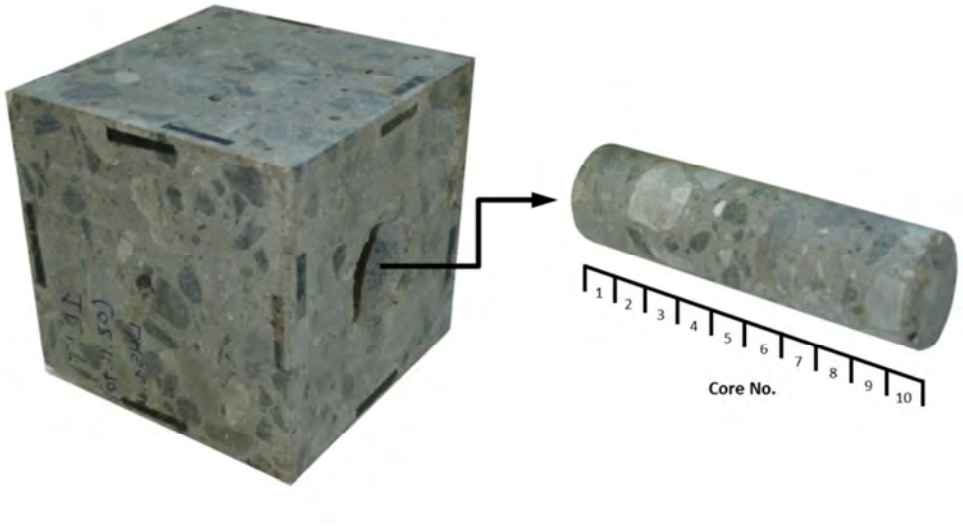

Figure 2: Schematic showing location and nomenclature of disks removed from concrete cube specimens.

Mercury Intrusion Porosimetry

MIP was carried out on disks 3, 7 and 8 (Figure 2) from each of the six cores. These disks were weighed and then heated at 105 ^{o}C until a constant weight was achieved, in order to remove any free water remaining in the concrete pore structure that may influence mercury intrusion. In all cases this took no longer than three days. Following heating the specimens were cooled and stored in a vacuum desiccator until testing. It has been reported that the heat treatment of concrete specimens at 105^{o}C causes significant changes to air void pore structure of the material (Stein *et al.* 2013). An increase in pore volume due to drying is therefore expected and this is likely to be most significant in control specimens. MIP experiments were carried out using a Poresizer 4000 from Micromeritics. The pressure range of this

equipment was between 0.006 and 200 MPa. Calculation of pore size distributions was undertaken using the Washburn equation (Washburn, 1921). A surface tension of 0.48 n/m^2 and a contact angle between mercury and solid material structure of 130^o were used in all calculations. Uncertainties reported are based on MIP testing of six disks for each conditioning regime, and are given with respect to the mean.

Backscattered Electron Imaging

Disk 5 from one specimen in each conditioning regime was prepared for SEM analysis according to Wong *et al.* (2006, 1). Each disk was vacuum-impregnated with a low viscosity epoxy resin and then polished using silicon carbide papers to 1200 grit. The resin blocks were then polished to a 1μm finish, using a non-aqueous diamond abrasive fluid. After polishing, the samples were cleaned in an ultrasonic bath using acetone and coated with a layer of carbon using an evaporative coater.

Images were obtained using a Zeiss Evo 50 tungsten filament scanning electron microscope fitted with a backscattered electron (BSE) detector. An accelerating voltage of 20 kV and a working distance of 7 mm were found to yield optimum image contrast. Thirty images with a magnification of 500x were collected from within the cementitious matrix of each disk. In accordance with Wong *et al.* (2006, 1), images were obtained in an equally spaced grid pattern in order to capture features such as the bulk cement paste and interfacial transition zone (ITZ) with a frequency representative of their contribution to volume fraction and aggregate distribution in an unbiased manner. The images were stored with a resolution of 1024 x 768 pixels, giving a field of view of 512 μm x 384 μm and a pixel size of 0.5 μm^2.

Image Analysis

The contribution of aggregate to total surface area in each BSE image varies significantly. A routine to enable the calculation of the volume fraction of pores in the binder phase was used for data acquisition. This procedure was achieved by adapting the method of Yang & Buenfeld (2001) through the use of a Canny edge detection algorithm implemented in Matlab in place of the gradient method used by the aforementioned authors. Porosity within the aggregate itself is also removed as this is not expected to contribute to any LITD which may be observed. An example of aggregate segmentation is shown in Figure 3.

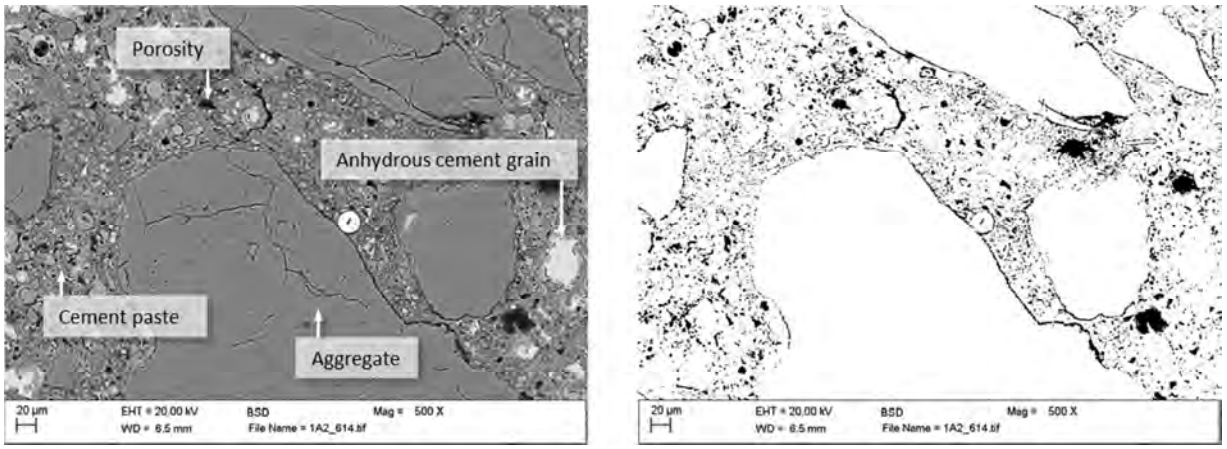

Figure 3: (left) Typical BSE image with principal phases highlighted (right) Segmented porosity in the cement paste.

The porosity of the binder phase was calculated from the processed images using the method of Wong *et al.* (2006, 2). It is assumed that the volume fraction of porosity in the concrete analysed here is

equivalent to its area fraction observed in the combined BSE images. Since no individual peak exists for voxels corresponding with the porous phase in the greyscale histogram of these images, simple minima thresholding cannot be utilized. The threshold greyscale level for porosity was instead determined from the point of inflection of the cumulative greyscale intensity plot. Termed the point of "overflow" (Wong *et al.* 2006, 2), this represents the value where a small increase in the threshold greyscale will yield a sudden increase in segmented porosity. Experimental error was determined by studying the influence of the number of SEM images on the statistical variation of results. For this experiment 20 images produced a stable value of porosity. This is in line with the number of images used by Wong *et al.* (2006, 1) for the analysis of mortar specimens.

RESULTS

Mercury Intrusion

Table 3 shows the total porosity and standard deviation for each of the three conditioning regimes. It is observed that both the H250 and the L06H250 (LITS affected) specimens experience a significant increase in total porosity of approximately 2.5% with respect to the control specimens. This is in line with experimental evidence provided by Xu *et al.* (2001) who performed MIP analysis on OPC-PFA specimens heated to 250 ^{O}C. The presence of load during heating does not appear to yield any significant alteration in total porosity.

Table 3: Porous volume results (total porosity) from MIP analysis of conditioned specimens.

	Control	**H250**	**L06H250**
Porous Volume (Standard deviation)	7.60 (0.71)	10.18 (0.90)	10.58 (1.66)

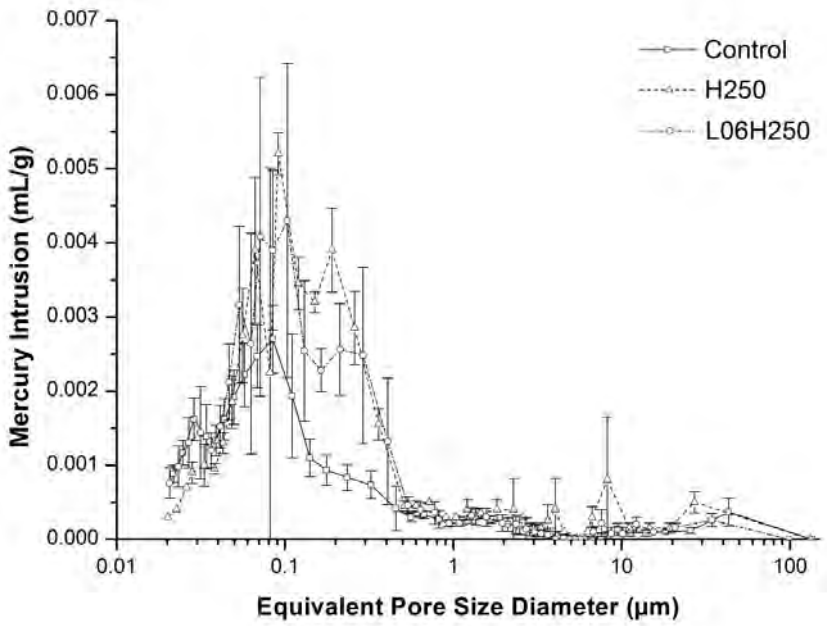

Figure 4: Pore size distribution of conditioning regimes as measured by MIP and the Washburn equation.

The pore size distribution of each of the three conditioning regimes as measured by MIP is shown in Figure 4. Interestingly, at pore sizes of below 1 μm in equivalent diameter both the H250 and L06H250 (LITS affected) specimens show a significant increase in measured pore volume compared to the control sample, concurrent with an increase in the variability of results indicated by standard deviation error bars. This may be the effect of increased permeability associated with the increase in porosity due to heating.

Differences between the pore size distribution results of H250 and L06H250 (LITS affected) are also visible. Between 0.02 and 0.05 μm the quantity of pores in the H250 regime appear suppressed. This contrasts with the presence of pores between 0.1 and 0.5 μm, where pores in the L06H250 (LITS affected) specimens seemed to be suppressed with respect to H250 specimens. Variation in the results for the control regime are reasonably consistent across the range of equivalent pore diameters, implying that the microstructural effects of thermal loading are heterogeneous and localized. However, the geometry of the pore structure can also have a large impact on the pore size distribution measured using this technique (Kaufmann, 2009).

Image Analysis

A typical BSE image from each of the 3 conditioning regimes is shown in Figure 5. The images show an appreciable difference in the homogeneity of the bulk cement paste between the H250 conditioning regime and both the L06H250 (LITS affected) and control regimes. A densification of the cement paste surrounding anhydrous cement particles in the H250 specimen microstructure is clearly present, indicated by lower porosity in these areas. A qualitative reduction in the size of anhydrous cement grains is also visible in the H250 specimens. However, in locations away from anhydrous cement grains, no apparent differences to similar areas in the L06H250 and control regimes could be observed.

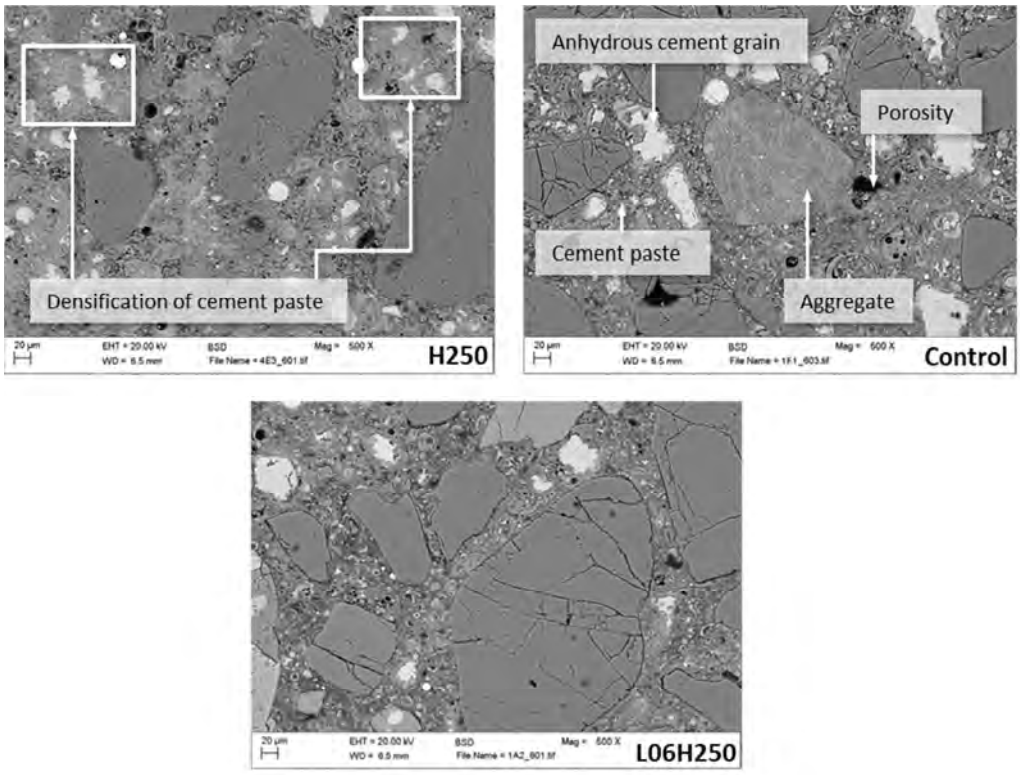

Figure 5: Typical BSE images from each of the conditioning regimes indicating features of interest.

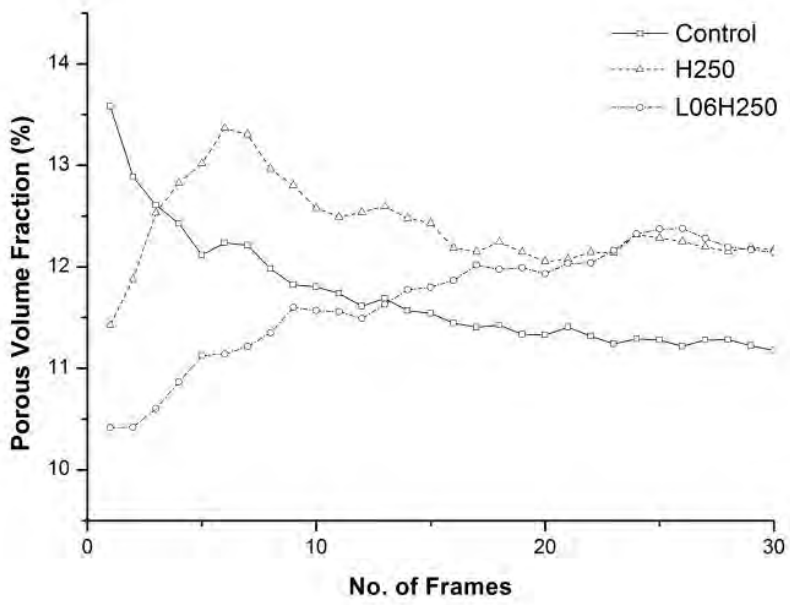

Figure 6: Variation of average total porosity with number of frames analysed. After twenty frames a relatively stable value of porosity was obtained.

Figure 6 shows the convergence of average paste porosity in accordance with the number of BSE images analysed, highlighting that approximately 20 images yield a stable estimate of porosity thereby indicating that the acquisition of additional images would not significantly affect the measurements presented here. The control specimen had a mean total porosity of 11%, and the paste porosity of the H250 and L06H250 specimens are around 1.5% higher. This trend agrees with the measurements recorded from MIP analysis here and in the work of Xu *et al.* (2001).

DISCUSSION

From MIP and BSE image analysis it is clear that both H250 and L06H250 (LITS affected) conditioning regimes experience an increase in volume fraction of porosity with respect to the unconditioned loading regime. The image analysis technique does however yield values for porosity slightly higher than those reported using the MIP technique. This is in contrast to the results of *Wong et al.* (2006, 1) who compared their image analysis results of cement mortars to those on cement paste using MIP by Cook & Hover (1999). Wong *et al.* found that the image analysis technique gave significantly lower values, since it allowed only for the analysis of pores with a size greater than the image resolution. This limitation on image analysis is also valid in the present case. One explanation for this contradiction may stem from the significantly greater volume of aggregate within specimens used in our investigation. Pixels belonging to aggregate particles are removed from the pore volume calculation and the values therefore represent the porosity of the cement matrix only. This may result in the artificial inflation of the image analysis results with respect to MIP results where the contribution of the aggregate to the solid phase is included.

This account does however not provide an explanation for the difference in pore volume recorded between the control and both heated specimens using each technique. MIP results indicate a ~2.5% increase and image analysis only a ~1.5% increase. In this case, microstructural damage caused by the application of thermal loading is likely to allow mercury intrusion into pore space which is disconnected

in the control specimens. Image analysis would not be susceptible to the aforementioned pore connectivity phenomenon and therefore the difference between the porosity of control and heated specimens would be reduced.

The MIP equipment utilised in this study is capable of detecting pores of >0.02 μm in diameter. Considering that similar trends in pore volume of the H250 and L06H250 conditioning regime are detected in the results from both analysis techniques employed here, no indication of the presence of the LITD mechanism appears to be present. However, the standard deviation in the results from MIP analysis of the L06H250 (LITS affected) specimens with respect to mean porous volume show a significant increase over that of the H250 and control specimens. This may indicate that the microstructural damage caused by heating results in much greater microstructural heterogeneity under the presence of a confining force.

CONCLUSIONS

MIP and SEM-based image analysis techniques were used to investigate the porous volume fraction within an OPC-PFA concrete which was subjected to combined thermal and mechanical loading in order to induce LITS. When compared with a specimen that had experienced heating only, no evidence was found to suggest that LITS resulted in an increase in porous volume. Specimens which experienced elevated temperatures did however show an increase in porosity when compared with those of the unconditioned control regime. Further investigation is required to determine if the variation in heterogeneity between H250 and L06H250 (LITS affected) microstructures suggested in the MIP pore size distribution data is a true material property. This will be carried out through the utilization of additional 2D image analysis techniques and 3D X-ray Computed Tomography.

REFERENCES

Anderberg, Y. & Thelandersson, S. (1976). "Stress and deformation characteristics of concrete: experimental investigation and material behaviour model". *University of Lund, Sweden*, Bulletin 5.

Bazant, Z. & Chern, J. (1985). "Concrete creep at variable humidity: constitutive law and mechanism". *Materials and structures*, 18(1), pp.1–20.

Cook, R.A. & Hover, K.C. (1999). "Mercury porosimetry of hardened cement pastes". *Cement and Concrete Research*, 29, pp.933–943.

Hansen, T.C. & Eriksson, L. (1966). "Temperature change effect on the behaviour of cement paste, mortar and concrete under load". *Journal of the American Concrete Institute*, 63(4), pp.489–504.

Kaufmann, J. (2009). "Characterization of Pore Space of Cement-Based Materials by Combined Mercury and Wood's Metal Intrusion". *Journal of the American Ceramic Society*, 92(1), pp.209–216.

Khoury, G.A. (1992). "Compressive strength of concrete at high temperatures: a reassessment". *Magazine of Concrete Research*, 44(161), pp.291–309.

Petkovski, M. (2010). "Effects of stress during heating on strength and stiffness of concrete at elevated temperature". *Cement and Concrete Research*, 40(12), pp.1744–1755.

Petkovski, M. & Crouch, R. (2008). "Strains under transient hygro-thermal states in concrete loaded in multiaxial compression and heated to 250 °C". *Cement and Concrete Research*, 38(4), pp.586–596.

Petkovski, M., Crouch, R.S. & Waldron, P. (2006). "Apparatus for Testing Concrete under Multiaxial Compression at Elevated Temperature (mac^{2T})". *Experimental Mechanics*, 46(3), pp.387–398.

Stein, R.C., Petkovski, M., Engelberg, D. L., Leonard, F., & Withers, P.J. (2013). "Characterizing the effects of elevated temperature on the air void pore structure of advanced gas-cooled reactor pressure vessel concrete using x-ray computed tomography". *European Physics Journal - Proceedings*, Accepted for Publication.

Washburn, E. (1921). "The dynamics of capillary flow". *Physical review*, 17(3), pp.273–284.

Wong, H.S., Buenfeld, N.R. & Head, M.K. (2006, 1). "Estimating transport properties of mortars using image analysis on backscattered electron images". *Cement and Concrete Research*, 36(8), pp.1556–1566.

Wong, H.S., Head, M.K. & Buenfeld, N.R. (2006, 2). "Pore segmentation of cement-based materials from backscattered electron images". *Cement and Concrete Research*, 36(6), pp.1083–1090.

Xu, Y., Wong, Y., Poon, C.S. & Anson, M., (2001). "Impact of high temperature on PFA concrete". *Cement and Concrete Research*, 31, pp.1065–1073.

Yang, R. & Buenfeld, N R. (2001). "Binary segmentation of aggregate in SEM image analysis of concrete". *Cement and Concrete Research*, 31(July 2000), pp.437–441.